X-RAY FLASHES FROM OFF-AXIS GAMMA-RAY BURSTS

RYO YAMAZAKI
Department of Physics, Kyoto University, Kyoto 606-8502, Japan; yamazaki@tap.scphys.kyoto-u.ac.jp

KUNIHITO IOKA
Department of Earth and Space Science, Osaka University, Toyonaka 560-0043, Japan; ioka@vega.ess.sci.osaka-u.ac.jp

AND

TAKASHI NAKAMURA[1]
Yukawa Institute for Theoretical Physics, Kyoto University, Kyoto 606-8502, Japan; takashi@yukawa.kyoto-u.ac.jp

ABSTRACT

K. Ioka and T. Nakamura proposed a simple jet model that is compatible with the peak luminosity–spectral lag relation, the peak luminosity–variability relation, and various other relations in the gamma-ray bursts. If the viewing angle is much larger than the collimation angle of the jet in the model by Ioka and Nakamura, for appropriate model parameters we obtain the observational characteristics of the X-ray flashes, such as the peak flux ratio and the fluence ratio between the γ-ray (50–300 keV) and the X-ray (2–10 keV) band, the X-ray photon index, the typical duration, and the event rate, ~ 100 yr^{-1}. In our model, if the distance to the X-ray flashes is much larger than ~ 1 Gpc (or $z \gtrsim 0.2$) they are too dim to be observed, so the spatial distribution of the X-ray flashes should be homogeneous and isotropic.

Subject headings: gamma rays: bursts — gamma rays: theory

1. INTRODUCTION

Recently, a new class of X-ray transients has been recognized. The Wide Field Cameras (WFCs) on *BeppoSAX* in the X-ray range 2–25 keV have detected some fast X-ray transients (FXTs) with a duration less than $\sim 10^3$ s, which are not triggered and not detected by the Gamma-Ray Burst Monitor (GRBM) in the γ-ray range 40–700 keV (Heise et al. 2001; see also Strohmayer et al. 1998; Gotthelf, Hamilton, & Helfand 1996; Hamilton, Gotthelf, & Helfand 1996). In Heise et al. (2001), these FXTs are defined as X-ray flashes (XRFs). This definition of XRFs excludes the X-ray counterparts of the typical gamma-ray bursts (GRBs) including X-ray–rich GRBs. Seventeen XRFs have been observed in the WFCs on *BeppoSAX* in about 5 yr, while 49 GRB counterparts have been observed in the same period.

XRFs have the following properties (Heise et al. 2001): (1) The peak flux of the XRFs ranges between 10^{-8} and 10^{-7} ergs s^{-1} cm^{-2} (Fig. 2 of Heise et al. 2001). The mean peak flux of the XRFs is about a factor of 3 smaller than that of the GRBs. Nine out of 17 XRFs are detected in either the lowest or the lowest two BATSE energy channels (25–50 and 50–100 keV; Kippen et al. 2001). (2) The ratio of the peak flux and the fluence in the X-ray range (2–10 keV) and the γ-ray range (50–300 keV) for nine XRFs are shown in Fig. 3 of Heise et al. (2001). The peak flux ratio extends up to a factor of 100, and the fluence ratio extends up to a factor of 20. (3) The energy spectrum in the range 2–25 keV fits with a single power law with the photon index between 1.2 and 3 and the mean of about 2, while the mean photon index of 36 GRBs in the same X-ray band is about 1, with the range between 0.5 and 3. (4) The duration of the XRFs ranges between 10 and 200 s, which is the same order as that of the GRBs. (5) The event rate of the XRFs is estimated as ~ 100 yr^{-1} since the WFCs observed ~ 3 yr^{-1} with the covering $40° \times 40°$ (full width to zero response). (6) The sky distribution is consistent with being isotropic. The spatial distribution is con-

sistent with being homogeneous in Euclidean space since $\langle V/V_{\max} \rangle = 0.56 \pm 0.12$ (J. Heise, J. in 't Zand, R. M. Kippen, R. D. Preece, P. M. Woods, & M. Briggs 2000, unpublished; Schmidt, Higdon, & Hueter 1988).

At present, the origin of the XRFs is not known. Heise et al. (2001) have proposed that XRFs could be GRBs at large redshift, $z > 5$, when γ-rays would be shifted into the X-ray range. However, as they have pointed out in their paper, one cannot explain the duration distribution since no time dilation due to cosmological expansion is observed. There is also a possibility that the XRFs could be dirty fireballs or failed GRBs (e.g., Dermer, Chiang, & Böttcher 1999; Heise et al. 2001; Huang, Dai, & Lu 2002).

Ioka & Nakamura (2001) have proposed that the XRFs could be GRBs observed from the large viewing angle as shown in Figure 1 (see also Nakamura 2000). They computed the kinematical dependence of the peak luminosity, the pulse width, and the spectral lag of the peak luminosity on the viewing angle θ_v of a jet. For appropriate model parameters, they obtained a peak luminosity–spectral lag relation similar to the observed one. They suggested that the viewing angle of the jet might cause various relations in GRBs, such as the peak luminosity–variability relation and the luminosity-width relation. Very recently, several authors have also suggested that the viewing angle is the key parameter to understanding the various properties of the GRBs (Zhang & Mészáros 2001; Rossi, Lazzati, & Rees 2002; Salmonson & Galama 2002). In this circumstance, it is meaningful to study the off-axis GRB model for the XRFs by Ioka & Nakamura (2001) in more detail.

In this Letter, we will show that the GRBs observed from the large viewing angle possess the above-mentioned properties 1–6 of the XRFs. In § 2, we describe a simple jet model for the XRFs. In § 3, we consider the peak flux ratio and the fluence ratio (property 2). In § 4, we consider the peak flux, the photon index, and the event rate (properties 1, 3, and 5). Section 5 is devoted to a discussion (properties 4 and 6).

[1] Present address: Department of Physics, Kyoto University, Kyoto 606-8502, Japan.

X−ray flash

θ_v

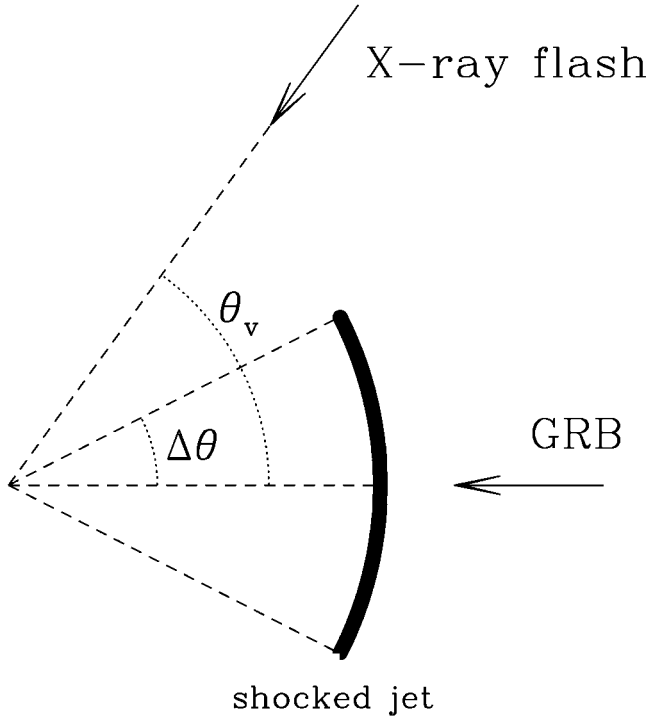$\Delta\theta$

GRB

shocked jet

Fig. 1.—Our model is schematically shown. The X-ray flashes are typical GRBs observed from the large viewing angle.

2. EMISSION MODEL OF X-RAY FLASHES

We apply the simple jet model by Ioka & Nakamura (2001) to XRFs. There are three timescales that determine the temporal pulse structure of XRFs: the hydrodynamic timescale T_{dyn}, the cooling timescale T_{cool}, and the angular spreading timescale T_{ang} (Kobayashi, Piran, & Sari 1997; Katz 1997; Fenimore, Madras, & Nayakshin 1996). Since we consider that XRFs are GRBs observed from the large viewing angle, we assume $T_{cool} \ll T_{dyn} \ll T_{ang}$ as in the case of GRBs (e.g., Piran 1999; Sari, Narayan, & Piran 1996). We adopt an instantaneous emission of an infinitesimally thin shell at $t = t_0$ and $r = r_0$. Then the observed flux of a single pulse at the observed time T is given by

$$F_\nu(T) = \frac{2c^2\beta\gamma^4 A_0(r_0/c\beta\gamma^2)}{D^2} \frac{\Delta\phi(T)f\{\nu\gamma[1-\beta\cos\theta(T)]\}}{\{\gamma^2[1-\beta\cos\theta(T)]\}^2},$$

(1)

where $1 - \beta\cos\theta(T) = (c\beta/r_0)(T - T_0)$ and $T_0 = t_0 - r_0/c\beta$. The quantity A_0 determines the normalization of emissivity, and $f(\nu')$ represents the spectral shape (for details, see Ioka & Nakamura 2001, Granot, Piran, & Sari 1999, and Woods & Loeb 1999). Let the jet opening half-angle and the viewing angle be $\Delta\theta$ and θ_v, respectively (see Fig. 1). For $\Delta\theta > \theta_v$ and $0 < \theta(T) \le \Delta\theta - \theta_v$, $\Delta\phi(T) = \pi$; otherwise, $\Delta\phi(T) = \cos^{-1}\{[\cos\Delta\theta - \cos\theta(T)\cos\theta_v]/\sin\theta_v\sin\theta(T)\}$. For $\theta_v < \Delta\theta$, $\theta(T)$ varies from 0 to $\theta_v + \Delta\theta$ and from $\theta_v - \Delta\theta$ to $\theta_v + \Delta\theta$ for $\theta_v > \Delta\theta$. In the latter case, $\Delta\phi(T) = 0$ for $\theta(T) = \theta_v - \Delta\theta$. A pulse starts at $T_{start} = T_0 + (r_0/c\beta)\{1 - \beta\cos[\max(0, \theta_v - \Delta\theta)]\}$ and ends at $T_{end} = T_0 + (r_0/c\beta)[1 - \beta\cos(\theta_v + \Delta\theta)]$.

The spectrum of the GRBs is well approximated by the Band spectrum (Band et al. 1993). In order to have a spectral shape similar to the Band spectrum, we adopt the following form of

the spectrum in the comoving frame:

$$f(\nu') = \left(\frac{\nu'}{\nu_0'}\right)^{1+\alpha_B}\left[1 + \left(\frac{\nu'}{\nu_0'}\right)^s\right]^{(\beta_B-\alpha_B)/s},$$

(2)

where α_B (β_B) is the low- (high-) energy power-law index and s describes the smoothness of the transition between the high and low energy. In the GRBs, $\alpha_B \sim -1$ and $\beta_B \sim -3$ are typical values (Preece et al. 2000). Equations (1) and (2) are the basic equations to calculate the flux of a single pulse, which depends on 10 parameters for $\gamma \gg 1$, $\theta_v \ll 1$, and $\Delta\theta \ll 1$: $\gamma\nu_0'$, $\gamma\theta_v$, $\gamma\Delta\theta$, $r_0/c\beta\gamma^2$, T_0, α_B, β_B, s, D, and $\gamma^4 A_0$.

In order to study the dependence on the viewing angle θ_v, we fix parameters as $\gamma\Delta\theta = 10$, $\alpha_B = -1$, $\gamma\nu_0' = 300$ keV, $r_0/c\beta\gamma^2 = 10$ s, and $s = 1$, since typical GRBs have a break energy of ~300 keV (Preece et al. 2000) and a pulse duration of ~10 s. Other parameters, i.e., the viewing angle $\gamma\theta_v$, the high-energy power-law index β_B, and the distance D, are varied depending on circumstances.

We fix the amplitude $\gamma^4 A_0$ so that the isotropic γ-ray energy $E_{iso} = 4\pi D^2 S(20-2000\text{ keV})$ equals 10^{53} ergs when $\beta_B = -3.0$ and $\gamma\theta_v = 0$. Here $S(\nu_1-\nu_2) = \int_{T_{start}}^{T_{end}} F(T; \nu_1-\nu_2)dT$ is the fluence in the energy range $\nu_1-\nu_2$ and $F(T; \nu_1-\nu_2) = \int_{\nu_1}^{\nu_2} F_\nu(T)d\nu$ is the flux in the same energy range. The result is

$$A_0 = 1.2 \text{ ergs cm}^{-2}\text{ Hz}^{-1} \frac{E_{iso}}{10^{53}\text{ ergs}}\left(\frac{r_0/c\beta\gamma^2}{10\text{ s}}\right)^{-2}\left(\frac{\gamma}{100}\right)^{-4}.$$

(3)

Note that when we adopt $\gamma = 100$, the opening half-angle of the jet is similar to the observed one, $\Delta\theta \sim 0.1$, and the total energy corrected for geometry is comparable to the observed value, $(\Delta\theta)^2 E_{iso} \sim 10^{51}$ ergs (Frail et al. 2001).

3. PEAK FLUX RATIO AND FLUENCE RATIO

In this section, we calculate the peak flux ratio $R_{peak} = F_{peak}(2-10\text{ keV})/F_{peak}(50-300\text{ keV})$ and the fluence ratio $R_{fluence} = S(2-10\text{ keV})/S(50-300\text{ keV})$ and compare the results with observations.

Figure 2 shows the peak flux ratio R_{peak} and the fluence ratio $R_{fluence}$ as a function of the viewing angle $\gamma\theta_v$. When the viewing angle θ_v is larger than the opening half-angle $\Delta\theta$, both the peak flux ratio R_{peak} and the fluence ratio $R_{fluence}$ increase as the viewing angle $\gamma\theta_v$ increases. The ratios, R_{peak} and $R_{fluence}$, increase as the high-energy index β_B decreases.

We can understand this behavior as follows. As shown in the Appendix, the maximum frequency ν_{max} at which most of the radiation energy is emitted is estimated as $\nu_{max} \sim \nu_0'/\delta$, where $\delta \equiv \gamma[1 - \beta\cos(\theta_v - \Delta\theta)] \simeq [1 + \gamma^2(\theta_v - \Delta\theta)^2]/2\gamma$ is the Doppler factor and $\theta_v > \Delta\theta$. Thus, the maximum frequency ν_{max} decreases as the viewing angle increases. In the following, we consider two observation bands: the lower energy band, $\nu_1-\nu_2$ keV, and the higher energy band, $\nu_3-\nu_4$ keV. The maximum frequency ν_{max} is larger than the highest observed energy ν_4 (=300 keV in the present case) when $\gamma\theta_v < \gamma\theta_v^{(4)} \equiv \gamma\Delta\theta + (2\gamma\nu_0'/\nu_4 - 1)^{1/2}$. In this case, we observe the low-energy part of the Band spectrum in equation (2). Since the low-energy power-law index is $\alpha_B = -1$, the peak flux ratio $R_{peak} = F_{peak}(\nu_1-\nu_2\text{ keV})/F_{peak}(\nu_3-\nu_4\text{ keV})$ and the fluence ratio $R_{fluence} = S(\nu_1-\nu_2\text{ keV})/S(\nu_3-\nu_4\text{ keV})$ are given by $R_{peak} \sim R_{fluence} \sim (\nu_2/\nu_4)^{2+\alpha_B}$, where $\alpha_B > -2$. Similarly, when the maximum frequency ν_{max}
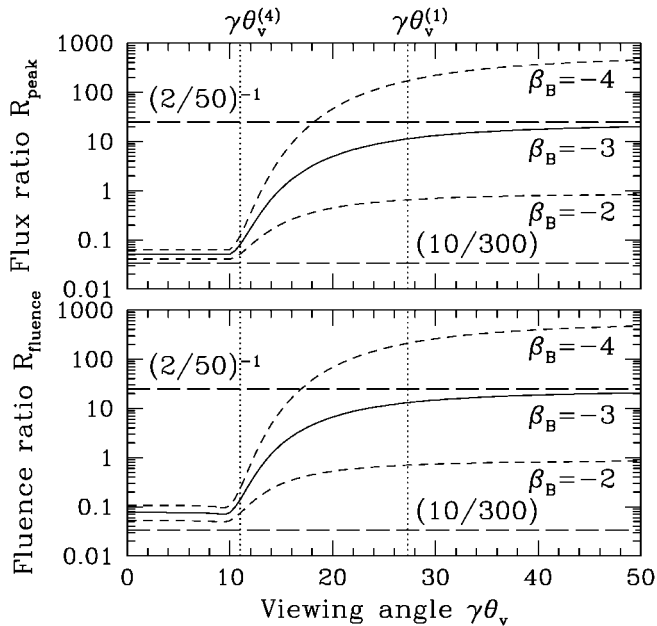
FIG. 2.—Peak flux ratio $R_{\rm peak} = F_{\rm peak}(2$–$10$ keV$)/F_{\rm peak}(50$–300 keV) (*upper panel*) and fluence ratio $R_{\rm fluence} = S(2$–10 keV$)/S(50$–300 keV) (*lower panel*) as a function of the viewing angle $\gamma\theta_v$. The solid curve shows the case $\beta_{\rm B} = -3$, and the dashed curves show the other cases, $\beta_{\rm B} = -2$ and $\beta_{\rm B} = -4$. We adopt $\gamma\Delta\theta = 10$, $\alpha_{\rm B} = -1$, $\gamma\nu'_0 = 300$ keV, and $s = 1$. The dotted line shows the viewing angle $\gamma\theta_v^{(1)} = 27.3$ ($\gamma\theta_v^{(4)} = 11$) at which the maximum frequency $\nu_{\rm max}$ equals the lowest (highest) observed energy, i.e., 2 keV (300 keV). Here the maximum frequency $\nu_{\rm max}$ means the frequency at which most of the radiation energy is emitted. At $\gamma\theta_v < \gamma\theta_v^{(4)}$ the ratios, $R_{\rm peak}$ and $R_{\rm fluence}$, nearly equal $(\nu_2/\nu_4)^{2+\alpha_{\rm B}} = 10/300$, and at $\gamma\theta_v > \gamma\theta_v^{(1)}$ the ratios, $R_{\rm peak}$ and $R_{\rm fluence}$, nearly equal $(\nu_1/\nu_3)^{2+\beta_{\rm B}} = (2/50)^{-1}$, as shown by the long-dashed lines.

is smaller than the lowest observed energy $\nu_1 = 2$ keV, i.e., $\gamma\theta_v > \gamma\theta_v^{(1)} \equiv \gamma\Delta\theta + (2\gamma\nu'_0/\nu_1 - 1)^{1/2}$, the peak flux ratio and the fluence ratio are given by $R_{\rm peak} \sim R_{\rm fluence} \sim (\nu_1/\nu_3)^{2+\beta_{\rm B}}$, where $\beta_{\rm B} < -2$.

We compare Figure 2 with observations. Observed peak flux ratios extend up to a factor of 100, and observed fluence ratios extend up to a factor of 20 (Fig. 3 of Heise et al. 2001). One can see that when $\gamma\Delta\theta = 10 \lesssim \gamma\theta_v \lesssim \gamma\theta_v^{(1)} \sim 3\gamma\Delta\theta$ and $-4 \lesssim \beta_{\rm B} \lesssim -2$, $R_{\rm peak}$ and $R_{\rm fluence}$ agree with the observational data. Furthermore, Kippen et al. (2002) reported that $\nu_{\rm max}$ ranges between about 2 and 90 keV. For our parameters, this can be reproduced if the viewing angle satisfies $\Delta\theta \lesssim \theta_v \lesssim \theta_v^{(1)}$.

4. PEAK FLUX, PHOTON INDEX, AND EVENT RATE

We calculate the peak flux and the photon index in the energy band 2–25 keV as a function of the viewing angle $\gamma\theta_v$ and plot it in the peak flux–photon index plane. Figure 3 shows the results for $\beta_{\rm B} = -3$. The distance is varied from $D = 0.01$ Gpc to $D = 2.1$ Gpc for our parameters.[2] One can see that the photon index increases and the peak flux decreases as the viewing angle $\gamma\theta_v$ increases.

As discussed in § 3, we observe the low- (high-) energy part of the Band spectrum in equation (2) when $\gamma\theta_v < \gamma\theta_v^{(4)}$ ($\gamma\theta_v > \gamma\theta_v^{(1)}$), where $\nu_4 = 25$ keV and $\nu_1 = 2$ keV. Therefore, the photon index in the energy range 2–25 keV is nearly equal to the low- (high-) energy spectral index $|\alpha_{\rm B}| = 1$ ($|\beta_{\rm B}| = 3$) when

---

[2] When we consider the effect of cosmology ($\Omega_M = 0.3$, $\Omega_\Lambda = 0.7$, and $h = 0.7$), $D \sim 2$ Gpc corresponds to $z \sim 0.4$. This does not affect our argument qualitatively but alters the quantitative results up to a factor of 2.
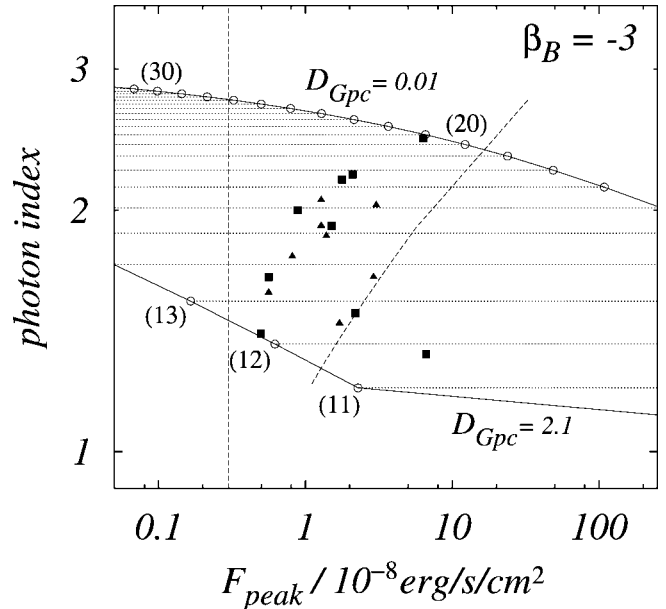

FIG. 3.—Photon index in the energy range 2–25 keV as a function of the peak flux in the same energy range by varying the distance D. We adopt $\gamma\Delta\theta = 10$, $\alpha_{\rm B} = -1$, $\beta_{\rm B} = -3$, $\gamma\nu'_0 = 300$ keV, and $s = 1$. The values of the viewing angle $\gamma\theta_v$ are given in parentheses. The right-hand side (left-hand side) of the two solid curves is $D = 0.01$ Gpc ($D = 2.1$ Gpc). Points that correspond to the same values of $\gamma\theta_v$ but different D are connected by horizontal dotted lines. The observed data shown are from Heise et al. (2001). Squares (triangles) are those which were (were not) detected by BATSE. The two dashed lines represent observational bounds. In the region to the left of the vertical dashed line, the peak flux in the X-ray band is smaller than the limiting sensitivity of WFCs ($\sim 3 \times 10^{-9}$ ergs s^{-1} cm^{-2}), and such events cannot be observed. In the region to the right of the oblique dashed line, the peak flux in the γ-ray band is larger than the limiting sensitivity of GRBM ($\sim 10^{-8}$ ergs s^{-1} cm^{-2}), and such events are observed as GRBs.

$\gamma\theta_v < \gamma\theta_v^{(4)} \simeq 14.8$ ($\gamma\theta_v > \gamma\theta_v^{(1)} \simeq 27.3$). With the analytical estimates in the Appendix, we can also find that the peak flux $F_{\rm peak}$ is approximately given by

$$F_{\rm peak} \simeq 4.3 \times 10^{-6} \ {\rm ergs \ s^{-1} \ cm^{-2}} \left(\frac{D}{1 \ {\rm Gpc}}\right)^{-2}$$

$$\times \ [1 + \gamma^2(\theta_v - \Delta\theta)^2]^{-2+\alpha_{\rm B}} \frac{r_0/c\beta\gamma^2}{10 \ {\rm s}}$$

$$\times \left(\frac{\gamma\nu'_0}{300 \ {\rm keV}}\right)^{-1-\alpha_{\rm B}} \frac{\gamma^4 A_0}{1.2 \times 10^8 \ {\rm ergs \ s \ cm^{-2}}} \quad (4)$$

when $\Delta\theta \lesssim \theta_v \lesssim \theta_v^{(4)}$. (In practice, eq. [4] can be applied to larger viewing angles $\gamma\theta_v \lesssim 30$. We have confirmed that numerical results can be fitted within 5% errors.)

The peak flux $F_{\rm peak}$ is smaller for larger viewing angles. However, if the distances to such sources are small, $F_{\rm peak}$ may be comparable to that of typical GRBs, which have large distances and small viewing angles.

For comparison, we also plot the observed data in the same figures (Fig. 2 of Heise et al. 2001). One can see that the observed XRFs take place within ~ 2 Gpc and have a viewing angle $\gamma\Delta\theta = 10 \lesssim \gamma\theta_v \lesssim \gamma\theta_v^{(1)} \sim 3\gamma\Delta\theta$.

We roughly estimate the limits in flux sensitivity of the detectors. On the right-hand side of the oblique dashed line, the peak flux in the γ-ray band $F_{\rm peak}(40$–700 keV) is larger than the limiting sensitivity of the GRBM ($\sim 10^{-8}$ ergs s^{-1} cm^{-2}),

and such events are observed as GRBs, not as XRFs. The vertical dashed line represents the limiting sensitivity of WFCs ($\sim 3 \times 10^{-9}$ ergs s^{-1} cm^{-2}). Therefore, the observed data of the XRFs sit in a fairly narrow region surrounded by two dashed lines.

The distance to the farthest XRF D_{XRF} gives the observed event rate of the XRFs. The observed event rate R_{XRF} can be estimated as $R_{\mathrm{XRF}} = r_{\mathrm{GRB}} n_g (4\pi D_{\mathrm{XRF}}^3/3)(f_{\mathrm{XRF}}/f_{\mathrm{GRB}})$, where r_{GRB} and n_g are the event rate of the GRBs and the number density of galaxies, respectively. The quantity f_{XRF} (f_{GRB}) is the solid angle subtended by the direction to which the source is observed as the XRF (GRB). From previous discussions, one can find that the emitting thin shell with opening half-angle $\Delta\theta$ is observed as the XRF (GRB) when the viewing angle is within $\Delta\theta \lesssim \theta_v \lesssim \theta_v^{(1)} \sim 3\Delta\theta$ ($0 \leq \theta_v \leq \Delta\theta$). Therefore, the ratio of each solid angle is estimated as $f_{\mathrm{XRF}}/f_{\mathrm{GRB}} \sim (3^2 - 1^2)/1^2 = 8$. Using this value, we obtain

$$R_{\mathrm{XRF}} \sim 10^2 \text{ events yr}^{-1} \frac{r_{\mathrm{GRB}}}{5 \times 10^{-8} \text{ events yr}^{-1} \text{ galaxy}^{-1}}$$

$$\times \left(\frac{D_{\mathrm{XRF}}}{2 \text{ Gpc}}\right)^3 \frac{n_g}{10^{-2} \text{ galaxies Mpc}^{-3}} \frac{f_{\mathrm{XRF}}/f_{\mathrm{GRB}}}{8}, \quad (5)$$

which is comparable to the observation.

5. DISCUSSION

We have shown that the observed data of XRFs can be reproduced by a simple jet model of GRBs. This suggests that XRFs are identical to GRBs. We may say that in the context of our model, nearby GRBs are observed as XRFs when we see them from the off-axis viewing angle. If the distance to the XRFs is much larger than a few gigaparsecs, they cannot be observed since the observed flux is low. This is consistent with the observed value of $\langle V/V_{\max}\rangle \sim 0.5$ since the nearby sources distribute homogeneously in Euclidean space.

Our view of XRFs is different from that of Heise et al. (2001). They have proposed that XRFs could be GRBs at large redshift, $z > 5$, when γ-rays would be shifted into the X-ray range. However, the observed total duration $T_{90}^{(\mathrm{obs})}$ cannot be explained. In our model, γ-rays are shifted into the X-ray range by the relativistic beaming effect. The total duration is equal to the lifetime of the central engine and thus does not depend

on the viewing angle θ_v. Hence, the total duration of the XRFs may be similar to that of the GRBs in our model.

We can calculate T_{90}, the observed duration of a single pulse in the X-ray band (2–25 keV). When the viewing angle ranges from $\gamma\theta_v = 10$ to $\gamma\theta_v = 30$, the pulse duration is about $T_{90} \sim 30$–3000 s [$(r_0/c\beta\gamma^2)/10$ s]. This value is comparable but a little bit inconsistent with the observation since the observed pulse duration T_{90}, which is on the order of the angular spreading timescale, should be less than the total duration $T_{90}^{(\mathrm{obs})} \sim 10$–200 s, which is the time interval between the first and the last emission. This contradiction can be resolved as follows. So far, we have assumed the isotropic energy of the instantaneous emission $E_{\mathrm{iso}} \sim 10^{53}$ ergs and the time unit $r_0/c\beta\gamma^2 \sim 10$ s. The effect of changing the values of these two parameters appears only in the flux normalization $(\gamma^4 A_0)(r_0/c\beta\gamma^2)$ in equation (1). However, one can see that from equation (3), if one rescales these parameters as $E_{\mathrm{iso}} \to E_{\mathrm{iso}}' = 10^{53}N^{-1}$ ergs and $r_0/c\beta\gamma^2 \to (r_0/c\beta\gamma^2)' = 10N^{-1}$ s, the flux normalization factor is invariant, $(\gamma^4 A_0)(r_0/c\beta\gamma^2) = [(\gamma^4 A_0)(r_0/c\beta\gamma^2)]'$, which implies that the result is unchanged. The value of N is the number of instantaneous emissions, since we fix the total emission energy as $E_{\mathrm{iso}}^{(\mathrm{tot})} = 10^{53}$ ergs. If we adopt $N \gtrsim 15$, T_{90} of each emission can be less than $T_{90}^{(\mathrm{obs})}$.

Ioka & Nakamura (2001) showed that the variability of GRBs is small for a large viewing angle. In addition, our model predicts that the number of pulses of XRFs is smaller than that of typical GRBs. This can be expected from the following discussion. In this Letter, we consider the time-averaged emissions, which means that successive emissions from multiple subjets with the opening half-angle $\Delta\theta^{(j)} \sim \gamma^{-1} \sim \Delta\theta/10$ are approximated by one spontaneous emission caused by a single jet with the viewing angle θ_v and the opening half-angle $\Delta\theta$. Let the viewing angle of each subjet be $\theta_v^{(j)}$. The observed flux (or fluence) in the X-ray band due to the subjets with $\theta_v^{(j)} \sim \theta_v + \Delta\theta$ is much smaller than that with $\theta_v^{(j)} \sim \theta_v - \Delta\theta$ and hence negligible. We have confirmed this in the practical calculation. If $\theta_v \gtrsim \Delta\theta$, the emissions of subjets with $\theta_v^{(j)} \sim \theta_v - \Delta\theta$ dominates, while if $\theta_v \sim 0$, in the GRB case, the emissions from almost all subjets may be detected.

APPENDIX A

ANALYTICAL ESTIMATES

$\nu_{\max}$ and $(\nu S_\nu)_{\max}$.—In equation (1), the typical value of $\theta(T)$ is $\sim(\theta_v - \Delta\theta)$ when $\theta_v > \Delta\theta$ since the flux peaks soon after the jet edge becomes visible. Since the function $\nu' f(\nu')$ in equation (2) takes a maximum at $\sim\nu_0'$, νS_ν takes a maximum at $\nu_{\max} \sim \nu_0'/\delta \propto \delta^{-1}$, where $\delta \equiv \gamma[1 - \beta \cos(\theta_v - \Delta\theta)] \simeq [1 + \gamma^2(\theta_v - \Delta\theta)^2]/2\gamma$ and $S_\nu = \int_{T_{\mathrm{start}}}^{T_{\mathrm{end}}} F_\nu(T)dT$. At $\nu_{\max}$, F_ν in equation (1) is proportional to δ^{-2} so that we expect $(\nu S_\nu)_{\max} \propto \delta^{-3}$ (Ioka & Nakamura 2001). Note here that $\int \Delta\phi(T)dT$ depends on θ_v and δ very weakly.

T_{ang} and $\nu F_\nu^{\mathrm{peak}}$.—The pulse duration T_{ang} can be estimated as $T_{\mathrm{ang}} \propto (T_{\mathrm{end}} - T_{\mathrm{start}}) \propto \theta_v^2 \propto \delta$ for $\theta_v \sim \Delta\theta$ and $T_{\mathrm{ang}} \propto (T_{\mathrm{end}} - T_{\mathrm{start}}) \propto \theta_v \propto \delta^{1/2}$ for $\theta_v \gg \Delta\theta$. The peak flux F_{peak} can be estimated from the relation $F_{\mathrm{peak}} T_{\mathrm{ang}} \sim S \propto \delta^{-1+\alpha_B}(\delta^{-1+\beta_B})$ when the maximum frequency $\nu_{\max}$ is higher (lower) than the observed frequency.

REFERENCES

Band, D., et al. 1993, ApJ, 413, 281
Dermer, C. D., Chiang, J., & Böttcher, M. 1999, ApJ, 513, 656
Fenimore, E. E., Madras, C. D., & Nayakshin, S. 1996, ApJ, 473, 998
Frail, D. A., et al. 2001, ApJ, 562, L55
Gotthelf, E. V., Hamilton, T. T., & Helfand, D. J. 1996, ApJ, 466, 779
Granot, J., Piran, T., & Sari, R. 1999, ApJ, 513, 679

Hamilton, T. T., Gotthelf, E. V., & Helfand, D. J. 1996, ApJ, 466, 795
Heise, J., in 't Zand, J., Kippen, R. M., & Woods, P. M. 2001, in Gamma-Ray Bursts in the Afterglow Era, ed. E. Costa, F. Frontera, & J. Hjorth (Berlin: Springer), 16
Huang, Y. F., Dai, Z. G., & Lu, T. 2002, MNRAS, 332, 735
Ioka, K., & Nakamura, T. 2001, ApJ, 554, L163
Katz, J. I. 1997, ApJ, 490, 633
Kippen, R. M., Woods, P. M., Heise, J., in 't Zand, J. J. M., Briggs, M. S., & Preece, R. D. 2002, preprint (astro-ph/0203114)
Kippen, R. M., Woods, P. M., Heise, J., in 't Zand, J. J. M., Preece, R. D., & Briggs, M. S. 2001, in Gamma-Ray Bursts in the Afterglow Era, ed. E. Costa, F. Frontera, & J. Hjorth (Berlin: Springer), 22
Kobayashi, S., Piran, T., & Sari, R. 1997, ApJ, 490, 92

Nakamura, T. 2000, ApJ, 534, L159
Piran, T. 1999, Phys. Rep., 314, 575
Preece, R. D., Briggs, M. S., Mallozzi, R. S., Pendleton, G. N., Paciesas, W. S., & Band, D. L. 2000, ApJS, 126, 19
Rossi, E., Lazzati, D., & Rees, M. J. 2002, MNRAS, in press (astro-ph/0112083)
Salmonson, J. D., & Galama, T. J. 2002, ApJ, in press (astro-ph/0112298)
Sari, R., Narayan, R., & Piran, T. 1996, ApJ, 473, 204
Schmidt, M., Higdon, J. C., & Hueter, G. 1988, ApJ, 329, L85
Strohmayer, T. E., Fenimore, E. E., Murakami, T., & Yoshida, A. 1998, ApJ, 500, 873
Woods, E., & Loeb, A. 1999, ApJ, 523, 187
Zhang, B., & Mészáros, P. 2001, AAS Meeting, 199, 12.01